

Why are we interested in angiography?

Diseases of the vascular system cause heart attacks, stroke, aneurysms, hypertension, poor perfusion. To fix the problems with the vascular system we need a way (minimally invasive if possible) to gain access to the vessels and to assess the success of the treatment. Angiography provides the means to view the vascular system. To obtain angiographic images, a catheter is inserted through an artery, (usually the femoral artery), and the catheter is guided through the arterial system using x-ray fluoroscopy, (relatively low dose acquisitions acquired usually at 30 frames per second projecting the imaged volume onto the image intensifier detector system (II)). Once the catheter is positioned proximal to the vessel regions of interest, digital images are acquired as x-ray absorbing contrast material is injected.

The basics of x-ray angiography

X-ray angiography is performed using full-field acquisition systems, consisting of a cathode-anode system, projection of the x rays through the object, and detection of the x rays with an image intensifier or flat panel detector system. Fluoroscopic imaging is used for interactive viewing, and digital acquisitions are used for assessments. The intensity at a given point on the detector is given by

$$I(x,y) = \exp(- \sum_E \sum_z I_0(x,y)_E \mu_E(x,y,z) \Delta z), \quad (1)$$

where $I_0(x,y)_E$ is the initial x-ray intensity at (x,y) at energy E , i.e., there is an energy spectrum to the x-ray beam, and $\mu_E(x,y,z)$ is the linear attenuation coefficient at position (x,y,z) . In general, we assume an average attenuation coefficient (weighted average) and a uniform x-ray intensity.

In angiography, contrast material is injected into the arteries replacing the blood. The contrast material has a higher attenuation coefficient than blood, so Eq. 1 becomes

$$I(x,y) = I_0 \exp(- \sum_{z=nc} \mu_{nc}(x,y,z) \Delta z_{nc} - \mu_c \Delta z_c) \quad (2)$$

where the subscripts nc and c refer to the non-contrast material tissue and the contrast material, respectively. By log conversion we have

$$\ln(I_0/I(x,y)) = - \sum_{z=nc} \mu(x,y,z) \Delta z - \mu \Delta z_c \quad (3)$$

Images are acquired before and after injection of contrast material and subtracted to yield the subtracted image,

$$I_s(x,y) = \mu \Delta z_c \quad (4)$$

The imaging system is characterized by the characteristic curve and the resolution of the imaging system. The characteristic curve expresses the relationship between the exposure (usually log relative exposure is used) and the optical density of the film or the pixel value in the digital image¹⁻³. The resolution of the imaging system is often expressed in terms of the modulation transfer function (MTF)⁴⁻⁶, which represents the response of the system to input at various frequencies.

Single Projection Angiography

In single projection angiography, x-rays are obtained, vessels are identified, vessel sizes are measured in the image either manually (say by clicking on the edges of the vessel) or using automated techniques applied to vessel profiles extracted from the image. Because only one projection has been obtained, a circular cross section for the vessel is assumed. It should be noted that Glagov, et al.⁷ have proposed a model for vascular disease in which the relative circularity of the vessel lumen is maintained as the lesion

grows, and Brown, et al.⁸ have indicated that approximately 96% of the luminal cross sections of stenosed coronary vessels are circular or elliptical. The techniques for automated measurement of vessel sizes fall into basically three categories, derivative-based⁹⁻¹⁴, densitometry-based¹⁵⁻¹⁶, and model-based¹⁷⁻¹⁹.

Derivative techniques measure distance between extrema in profile derivatives. These tend to yield accurate sizes for large vessels (if calibrated)

Densitometric techniques compare the area under the profile of the vessel of interest with the area under the profile from a vessel of known size. These techniques can yield accurate vessel sizes over a range of vessel diameters; they are relatively insensitive to the resolution function, but are sensitive to background estimation, angulation of the vessels, and linearization using the characteristic curve.

Model-based techniques assume a model for the vessel and take the resolution into account in some way. These techniques can yield accurate vessel sizes for vessels with elliptical cross sections but are sensitive to linearization using the characteristic curve and to modeling of resolution function.

In all the evaluations, the magnification was considered to be known exactly. In general, all techniques measure vessel sizes in the images and correct the measured sizes for magnification to obtain the diameter. The magnification is usually determined by measuring the size of the catheter in the image¹⁴. The errors in the size measurement, E_{size} , and the errors in the calculated magnification, E_{mag} , can be considered separately as a (good) first approximation, i.e.,

$$E_{\text{diam}} = E(\text{size/mag}) = \text{size/mag} * \sqrt{[(E_{\text{mag}}/\text{mag})^2 + (E_{\text{size}}/\text{size})^2]} + O[(E_{\text{mag}} * E_{\text{size}})/(\text{mag} * \text{size})] \quad (5)$$

where $O[x]$ stands for “of the order of x ”. Errors in the estimated vessel diameters would therefore have to include E_{size} as well as those resulting from errors in the estimated magnification. Orientations are usually not determined, but when determined, the distances between known points (with known distances) are measured. The relationship is a simple cosine relationship, i.e., $l_{\text{measured}} = l_{\text{true}} * \cos(\theta)$, where θ is the angle between the imaging plane and the axis of the calibration object.

Accuracies and reproducibilities

Sizes²⁰ 0.050 – 0.100 mm

Mag ~ 1%

Orientation ~ 2 degrees

Requirements/limitations

Linearization of system

Circular cross section assumed

Limited to vessel segments where magnification and orientation determined

Biplane 3D Angiography

In biplane angiography two prospective projection views of the vascular system are obtained. To determine the 3D vascular system from these two views the following steps are taken: the imaging geometry is determined, corresponding points in the two systems are determined, vessel profiles are extracted along epipolar lines, the system is linearized using the characteristic curve, the sizes are determined in both views, and then the lumen is reconstructed.

The two imaging systems (Fig. 1) are related to each other through a rigid body transformation, i.e.,

$$\mathbf{x}' = \mathbf{R}(\mathbf{x} - \mathbf{t}) \quad (6)$$

where \mathbf{R} and \mathbf{t} are the rotation matrix and translation vector, respectively, relating the two coordinate systems. The imaging geometry can be determined using calibration objects^{21,22} or by self-calibrating²³⁻²⁸.

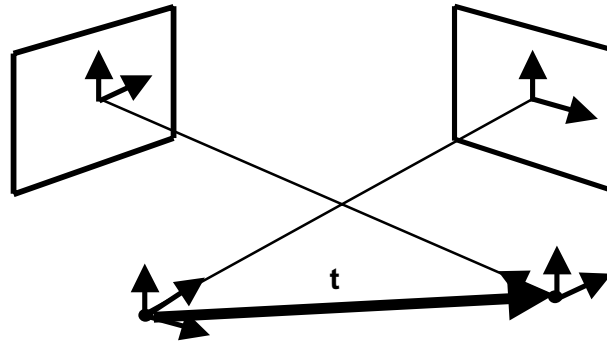


Figure 1. Biplane imaging system. Projections are obtained using x-rays from two focal spots onto the two image detector planes. The systems are related to each other through a rotation matrix, \mathbf{R} , and a translation vector, \mathbf{t} .

Once the geometry is determined, the corresponding points and regions along the vessels are determined. In general, the correspondence is not apparent, such as with bifurcation points, therefore, the correspondence is usually determined using epipolar lines^{21,22} (Figure 2).

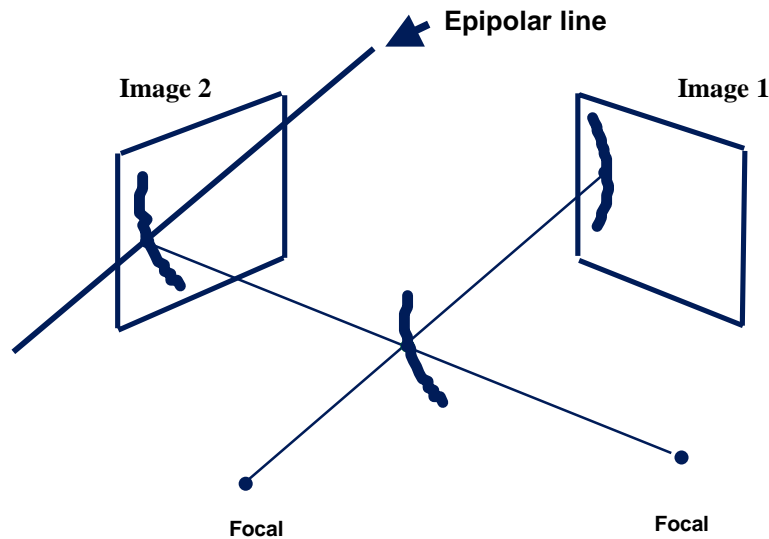


Figure 2. Illustration of the epipolar line. A point along one vessel in one image is identified, a line in 3D is drawn from this point back to its own focal spot, this line is projected into the second image using the determined geometry, i.e., the transformation between the two imaging systems. This line in the second image is called the epipolar line. The intersection of this epipolar line with the vessel axis in the second image is taken as the point which corresponds to the vessel point in the first image²⁹.

Similarly, a “corresponding” epipolar line can be generated in the first image using the determined point in the second image. Vessel profiles are extracted along the corresponding epipolar lines. These profiles can then be used to reconstruct vessel lumen. The sizes measured in the two images can be used to generate an elliptical cross section, this cross section can then be modified using the projection data³⁰⁻³⁴.

Evaluations of the reconstructed cross sections are still being developed, but some suggestions are comparison of true and reconstructed lumen, using overlapped regions or distance between boundaries³⁴.

Accuracies and reproducibilities

Imaging geometry/3D location

Mag	~ 1%
Orientation	~ 2 deg.
Position	~ 0.5 – 1 cm
Relative positions	~ 0.1 cm

Lumen reconstruction

99% overlap between original and reconstructed

Reconstruction using multiple projections

Three dimensional angiography has developed rapidly in the last few years, primarily because two substantial changes have occurred in computed tomography (CT) technology, i.e., helical CT and multi-detector technology. Prior to describing these two technological developments, let us consider some of the basic aspects of standard CT technology on which these are built.

CT technology is based on the **central axis theorem**. In parallel beam CT, projections of an object are acquired at many different angles.

$$P(x', \Theta) = \int p(x, y) dy' \quad (7)$$

where $p(x, y)$ is the distribution of the linear attenuation coefficient in the $z = \text{constant}$ plane, and the integration is along the y' direction (oriented at an angle of Θ relative to the y axis). A simple backprojection does not yield the correct result. This can be seen if we acquire a projection of a point object, then simply backproject. We obtain a spoke-like image with a maximum in the center. Although a simple thresholding would yield the correct result in this case, but these artifacts would obfuscate the actual data in the presence of multiple point-like objects, i.e., a human body. Another approach must be taken. Consider the following. The real space distribution can be represented by its Fourier transform.

$$p(x, y) = \int \rho(v_x, v_y) \exp(-iv_x x) \exp(-iv_y y) dv_x dv_y \quad (8)$$

$$P(x', \Theta) = \int \rho(v_x, v_y) \exp(-iv_x x) \exp(-iv_y y) dv_x dv_y dy' \quad (9)$$

Remember the delta function

$$\delta(v') = \int d\alpha \exp(-i\alpha v') \quad (10)$$

$$\int \int$$

$$\mathbf{P}(\mathbf{x},0) = \int \rho(v_x, v_y) \exp(-i\mathbf{v}_x \mathbf{x}) \left\{ \int \exp(-i\mathbf{v}_y \mathbf{y}) d\mathbf{y} \right\} dv_x dv_y \quad (11)$$

$$\mathbf{P}(\mathbf{x},0) = \int \rho(v_x, v_y) \exp(-i\mathbf{v}_x \mathbf{x}) \delta(v_y) dv_x dv_y \quad (12)$$

$$\mathbf{P}(\mathbf{x},0) = \int \rho(v_x, 0) \exp(-i\mathbf{v}_x \mathbf{x}) dv_x \quad (13)$$

Likewise

$$\rho(v_x, 0) = \int \mathbf{P}(\mathbf{x},0) \exp(i\mathbf{v}_x \mathbf{x}) d\mathbf{x} \quad (14)$$

Eq. 13 and 14 demonstrate the **central axis theorem**, i.e., that Fourier transforms of projections are samplings of the Fourier space distribution. Thus, every time you get a projection, you get a sample along a line in Fourier space of the Fourier distribution. If you get enough projections, you can fill up Fourier space, i.e., get the “entire” $\rho(v_x, v_y)$. With Fourier space sufficiently sampled, you can get the original distribution back by a Fourier transform of the Fourier space distribution, via equation 8. Unfortunately, there is a problem, the sampling is polar, i.e., the samples are obtained at uniform angular intervals. Thus, the polar nature of the data needs to be taken into account, either by interpolation onto a rectangular mesh or by using the polar Fourier transform

$$\mathbf{p}(\mathbf{x}) = \int \rho(\xi, \Theta) \exp(-i\xi \cdot \mathbf{x}) \xi d\xi d\Theta \quad (15)$$

where ξ is the radial coordinate in Fourier space and \mathbf{x} is now a vector. This factor ξ effectively multiplies the Fourier space coefficients, i.e., a “ramp” function which increases with frequency. Remember, multiplication in Fourier Space is a convolution in real space, so if we convolve the real space projections with the Fourier transform of the ramp function prior to backprojection, we get the right result! Now we are ready to go. Obtain projections from multiple angles in a given plane and properly backproject for in that plane. For single slice CT, move the patient after the acquisitions for a given slice have been completed, i.e., what I will call shoot-and-move CT.

What are the issues? Radial resolution determined by collimators, tangential resolution or sampling determined by angular sampling, sharp edges in one space produce ringing in reciprocal space, beam hardening (as the x-ray beam passes through the body, the lower energy x-rays are preferentially absorbed, thus the beam spectrum changes, becoming “harder” as the beam passes through the body), partial volume effects (the voxel value in the image is the weighted sum of the linear attenuation coefficients in that voxel). Resolution is approximately 0.5 – 1.0 mm in plane and 1.0 – 5 mm out of plane.

But perhaps the most important issue is that CT is not parallel beam, but rather fan beam. The fan beam nature can be taken into account by appropriately rebinning the data to effect a parallel beam geometry or the equation relating the projections and the Fourier transforms (i.e., equation 15) must be modified to take the fan beam geometry into account (effectively using the appropriate Jacobian)³⁵.

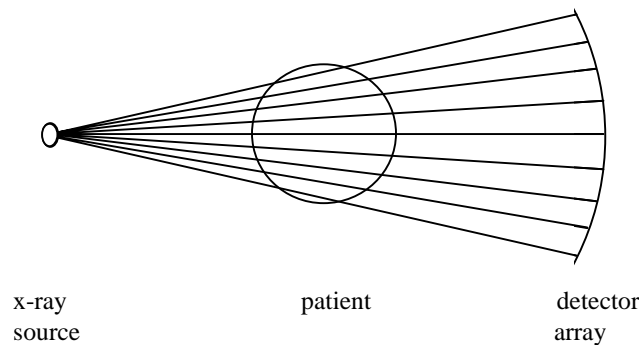


Figure 3. Fan beam geometry. X-rays propagate from a source which is a finite distance from the detector. The projection lines, rather than being parallel, diverge like a fan.

Although 3D angiography was possible with shoot-and-move CT, it was rarely used, the vessels, continuous in reality, looked like series of coins stacked up on each other often giving an unappealing and non-diagnostic staircase effect.

Helical CT

In the 1990's, a number of vendors introduced helical (or spiral) CT. In this technology, the patient was moved continuously while the x-ray tube and detectors rotated continuously about the patient. This approach had a number of advantages, the primary ones being that the speed of acquisition was increased and that arbitrary planes could be reconstructed. The latter resulted in the possibility of reconstructing the physically continuous structures (vessels in particular) so that they appeared more continuous. However, because the patient was moving during the acquisition, the data for a single plane was not acquired, rather created by interpolation. As indicated in Figure 4, the data is acquired along a helical path. The projection data for a given plane is interpolated from the data on the helical path using an interpolation scheme. The simplest interpolation scheme uses the weighted averaging of the data at the same angular position along the helix.

The distance between sequential helices, Δ , is known as the pitch. The symmetry of x-ray absorption can be taken advantage of, and the interpolation can also be performed between the parts of the helix separated by 180 degrees. By these interpolations, planes can be generated at arbitrary locations along the length of the helix. Simply stated, with helical scanning one effectively has a cylinder of projection data, from which projection data for arbitrary planes can be generated. Because the planes can be generated at arbitrary locations or distances along the helix and because interpolation is used, the continuity of the structures reconstructed is much greater than the shoot-and-move CT. As a result, blood vessels and other connected structures not only appear but are much more continuous.

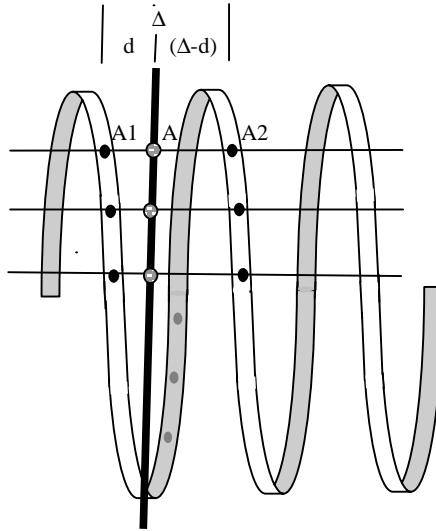


Figure 4. Schematic of Helical CT acquisition and interpolation. Projections (black dots, e.g., A1 and A2) are obtained as the x-ray-detector assembly rotates about a patient being moved along the axis of the helix at a fixed speed. Projection data (e.g., A) for a given plane are generated by interpolating the acquired data: in linear interpolation, $A = (1 - f) \cdot A1 + f \cdot A2$, where $f = d/\Delta$, where d is the distance between A1 and A, and Δ is the distance between A1 and A2, i.e., the pitch.

The in-plane resolution in the reconstructed images is determined by the collimators and angular sampling (as in shoot-and-move CT), but the out-of-plane resolution is the result of the collimator aperture and the table motion profile which depends on the pitch and the interpolation method used³⁵. The symmetry of x-ray absorption can be taken advantage of, and the interpolation can also be performed between the parts of the helix separated by 180 degrees. By these interpolations, planes can be generated at arbitrary locations along the length of the helix. Simply stated, with helical scanning one effectively has a cylinder of projection data, from which projection data for arbitrary planes can be generated. Because the planes can be generated at arbitrary locations or distances along the helix and because interpolation is used, the continuity of the structures reconstructed is much greater than the shoot-and-move CT. As a result, blood vessels and other connected structures not only appear but are much more continuous³⁶.

Multi-detector or cone-beam CT

By adding out-of-plane detectors, more projections can be obtained with each rotation of the CT gantry. Current clinical systems have as many as 16 rows of detectors. In addition, by rotating an x-ray-II system about the patient while contrast flows through the vessels being imaged, the entire vascular volume can be reconstructed. In the case of large out-of-plane distances, the fan-beam reconstruction algorithms need to be modified to take into account the out-of-plane projection geometry, similar to the parallel-beam-to-fan-beam modifications^{37,38}. The advantages of multi-detector CT are mainly reduced time of acquisition. Indeed, the speed of rotation has been increased so that an entire 360 degree sweep takes less than 0.5 seconds on at least one commercial system, and the acquisitions can be either prospectively or retrospectively gated so that only those acquisitions are used which occur during or near the diastolic phase of the heart cycle (about 200 milliseconds time window). As a result, images of the coronary vessels are being reconstructed³⁹.

It should be noted that image distortions and errors in the imaging geometry (e.g., wobbling of the gantry) need to be corrected or properly taken into account³⁸. The cone beam technology has, in general, higher resolution detectors than single slice or shoot-and-move CT; thus, the reconstructed vascular system has potentially fewer artifacts and is a better representation of the actual anatomy.

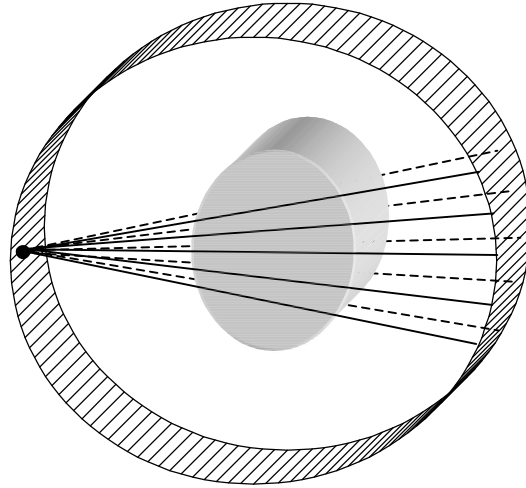


Figure 5 Illustration of multi-detector acquisition. X rays from a single source project in a diverging cone and are detected. In order to backproject into the proper voxel, the Feldkamp algorithm³⁷ (which takes the divergence into account) should be used.

3D vascular rendering and analysis

With the vascular data generated from multi-detector and cone-beam technology, the rendered vascular structures are more continuous and “believable”, in addition, they provide valuable data for subsequent analysis. Visualization tools, such as maximum intensity projections, surface rendering, and volume rendering, are being used more frequently in the diagnostic process. More and more analysis techniques are being developed to characterize the vascular system and its abnormalities. Moreover, by segmenting the vascular tree using simple to sophisticated region-growing techniques, the vascular tree is available for quantitative analysis and for image fusion across modalities^{40,41}.

Summary

Three-dimensional angiography can be performed using single, biplane, or multiple plane acquisitions. Each of these acquisition technologies require understanding of the information provided and its limitations. Single plane can give good circular vessel information (the vast majority of the vessel tree), if properly calibrated. Biplane acquisitions can yield the vessel lumen cross section throughout the vessel tree, elliptical as well as cross sections with asymmetries, once the geometry is properly calibrated. CT angiography is being used clinically ever more frequently, especially when multi-detector acquisitions are available with resolutions approaching that of II acquisition devices. The vascular tree rendered from such data sets is truly impressive in its detail.

Full-field angiography is still the modality of choice for interventional procedures, but 3D angiography is a powerful adjunct prior to and during the procedure. Patients will be well served as the power of each of these technologies (in terms of visualization and analysis) is combined during the diagnosis, during, and after the intervention.

Acknowledgments

Supported by USPHS grant number NIH HL-RO1-52567 and The Toshiba Corporation.

References

1. H. P. Chan, K. Doi: Determination of radiographic screen-film characteristic curve and its gradient by use of a curve-smoothing technique. *Med. Phys.* 5: 443-7, 1978.
2. D. R. Bednarek, S. Rudin: Computer-aided bootstrap generation of characteristic curves for radiographic imaging systems. *Med Phys.* 28: 515-20, 2001
3. H. Fujita, K. Doi, M. L. Giger, H. P. Chan: Investigation of basic imaging properties in digital radiography. 5. Characteristic curves of II-TV digital systems. *Med. Phys* 13: 13-18, 1986.
4. C. E. Metz, K. Doi: Transfer function analysis of radiographic imaging systems. *Phys. Med. Biol.* 24: 1079-1106, 1979.
5. Fujita, K. Doi, M. L. Giger: Investigation of basic imaging properties in digital radiography. 6. MTFs of II-TV digital imaging systems. *Med. Phys.* 12: 712-720, 1985.
6. H. Fujita, D. Y. Tsai, T. Itoh, K. Doi, J. Morishita, K. Ueda, A. Ohtsuka: A simple method for determining the modulation transfer function in digital radiography. *IEEE Tran. Med. Imag.* 11: 34-39, 1992.
7. S. Glagov, E. Weisenberg, C. K. Zarins, R. Stankunavicius, G. J. Kolettis: Compensatory enlargement of human atherosclerotic coronary arteries. *NE Jour. Med.* 316: 1371-1375, 1987.
8. B. G. Brown, E. L. Bolson, H. T. Dodge: Dynamic mechanisms in human coronary stenosis. *Circulation* 74: 106-111, 1986.
9. J. Haase, C. DiMario, C. J. Slager, W. J. van der Giessen, A. den Boer, P. J. deFeyter, J. H. Reiber, P. D. Verdouw, P. W. Serruys: In-vivo validation of on-line and off-line geometric coronary measurements using insertion of stenosis phantoms in porcine coronary arteries. *Cathet Cardiovasc Diagn* 27: 16-27, 1992.
10. P. M. van der Zwet, J. H. Reiber: A new approach for the quantification of complex lesion morphology: the gradient field transform; basic principles and validation results. *JACC* 24: 216-24, 1994.
11. R. L. Kirkeeide, P. Fung, R. W. Smalling, K. L. Gould: Automated evaluation of vessel diameter from arteriograms. *Comp in Cardio*: 215-218, 1982.
12. M. T. LeFree, S. B. Simon, G. B. J. Mancini, R. A. Vogel: Digital radiographic assessment of coronary arterial geometric diameter and videodensitometric cross-sectional area. *Proc. SPIE* 626, 334-??? 1986.
13. M. Sonka, G. K. Reddy, M. D. Winniford, S. M. Collins: Adaptive approach to accurate analysis of small-diameter vessels in cineangiograms. *IEEE TMI* 16: 87-95, 1997.
14. The reader is recommended to perform a literature search on J.H.C. Reiber to obtain any number of papers on vessel sizing in projection imaging using derivative techniques and aspects of it.
15. R. A. Kruger: Estimation of the diameter of and iodine concentration within blood vessels using digital radiography devices. *Med Phys* 8: 652-658, 1981.
16. M. A. Simons, R. A. Kruger, R. L. Power. Cross-sectional area measurements by digital subtraction videodensitometry. *Invest. Rad.* 8: 637-644, 1986.
17. H. Fujita, K. Doi, L. E. Fencil, K. G. Chua: Image feature analysis and computer-aided diagnosis in digital radiography. 2. Computerized determination of vessel sizes in digital subtraction angiographic images. *Med Phys* 14: 549-556, 1987.
18. D. M. Weber: Absolute diameter measurements of coronary arteries based on the first zero crossing of the Fourier spectrum. *Med. Phys.* 16: 188-196, 1989.
19. R. C. Chan, W. C. Karl, R. S. Lee: A new model-based technique for enhanced small-vessel measurement in x-ray cine-angiograms. *IEEE Trans. Med. Img.* 19: 243-255, 2000.
20. Hoffmann KR, Nazareth DP, Miskolczi L, Gopal A, Wang Z., Rudin S, Bednarek D: Vessel size measurements in angiograms: a comparison of automated techniques. *Medical Physics* (in press).
21. M. J. Potel, J. M. Rubin, S. A. MacKay, A. M. Aisen, J. Al-Sadir, and R. E. Sayre: Methods for evaluating cardiac wall motion in three dimensions using bifurcation points of the coronary arterial tree. *Invest Radiol* 8: 47-57, 1983.
22. D. Parker, D. Pope, R. Van Bree, and H. Marshall: Three-dimensional reconstruction of moving arterial beds from digital subtraction angiography. *Comp. and Biomed. Res.* 20: 166-185, 1987.

23. C. E. Metz and L. E. Fencil: Determination of three-dimensional structure in biplane radiography without prior knowledge of the relationship between the two views. *Med Phys* 16: 45-51, 1989.
24. K. R. Hoffmann, C. E. Metz, Y. Chen: Determination of 3D imaging geometry and object configurations from two biplane views: an enhancement of the Metz-Fencil technique. *Med Phys* 22: 1219-1227, 1995.
25. A. Wahle, E. Wellnhofer, I. Mugaragu, H. U. Sauer, H. Oswald, and E. Fleck: Assessment of diffuse coronary artery disease by quantitative analysis of coronary morphology based upon 3-D reconstruction from biplane angiograms. *IEEE Transactions on Medical Imaging* 14: 230-241, 1995.
26. S. Y. J. Chen, C. E. Metz: Improved determination of biplane imaging geometry from two projection images and its application to three-dimensional reconstruction of coronary arterial trees. *Med. Phys.* 24: 633-654, 1997.
27. C. J. Henri, T. M. Peters: Three dimensional reconstruction of vascular trees. Theory and methodology. *Med Phys.* 23: 197-204, 1996.
28. R. Close, C. Morioka, J. S. Whiting: Automatic correction of biplane projection imaging geometry. *Med Phys* 23: 133-139, 1996.
29. Hoffmann KR, Sen A, Lan L, Chua KG, Esthappan J, Mazzucco M. A system for determination of 3D vessel trees from biplane images. *Int J Card Imaging* 16:315-330, 2000.
30. Hoffmann KR, Wahle A, Pellot-Barakat C, Sklansky J, Sonka M: Biplane x-ray angiograms, intravascular ultrasound, and 3D visualization of coronary vessels. *Int J Card Imaging* 15: 495-512, 1999 and references contained therein.
31. Y. Bresler and A. Macovsky: Estimation of the 3D shape of blood vessels from X-Ray Images. *Proc. IEEE Comput. Soc. Int. Symp. Med. Images Icons*, Arlington, Texas: 251-258, 1984.
32. C. Pellot, A. Herment, M. Sigelle, P. Horain, P. Peronneau: Segmentation, modeling, and reconstruction of arterial bifurcations in digital angiography. *Med. & Biol. Eng. & Comp.* 30: 576-583, 1992.
33. C. Pellot, A. Herment, M. Sigelle, P. Horain, H. Maitre and P. Peronneau: A 3D reconstruction of vascular structures from two x-ray angiograms using an adapted simulated annealing algorithm. *IEEE Transactions on Medical Imaging* 13: 48-60, 1994.
34. Gopal A, Hoffmann KR, Rudin S, Bednarek DR: Reconstruction of Asymmetric Vessel Lumen from Two Views. *Proc. SPIE* (in press).
35. The reader is recommended to perform a literature search on W. A. Kalender, J. Hsieh, or X. Pan to obtain any number of papers on CT reconstruction and aspects of it.
36. The reader is recommended to perform a literature search on "CTA visualization" to obtain any number of papers on CT angiography and aspects of it.
37. Feldkamp LA, Davis LC, Kress JW: Practical Cone Beam Algorithm. *J. Opt. Soc. Amer.* 1, 612-619, 1984.
38. The reader is recommended to perform a literature search on cone beam CT or R. Fahrig, D. Holdsworth, R. Ning, M. Grass for useful articles on experience with cone beam reconstruction.
39. M. Heuschmid, A. Kuttner, T. Flohr, J. E. Wildberger, M. Lell, A.F. Kopp, S. Schroder, U. Baum, S. Schaller S, A. Hartung, B. Ohnesorge, C.D. Claussen. Visualization of coronary arteries in CT as assessed by a new 16 slice technology and reduced gantry rotation time: first experiences. *Rofo Fortschr Geb Rontgenstr Neuen Bildgeb Verfahr.* 174:721-4, 2002. German.
40. G. P. M. Prause, S. C. DeJong, C. R. McKay, and M. Sonka: Semi-automated segmentation and 3-D reconstruction of coronary trees: Biplane angiography and intravascular ultrasound data fusion. *Proc. SPIE* 2709: 82-92, 1996.
41. The reader is recommended to perform a literature search on M. Sonka for papers on fusion of ultrasound and biplane angiography and aspects of it.